Analysis of CO_2 frost formation properties in cryogenic capture process

Chun-Feng Song [1], Yutaka Kitamura [1*], Shu-Hong Li [1], Wei-Zhong Jiang [2]

[1] *Graduate School of Life and Environmental Sciences, University of Tsukuba, 1-1-1, Tennodai, Tsukuba, Ibaraki 305-8572, Japan*

[2] *Key Laboratory of Agricultural Engineering in Structure and Environment, Ministry of Agriculture, China Agricultural University, Qinghua Donglu 17, Beijing 100083, China*

* Corresponding author. Tel.: +81 0298-53-4655; Fax: +81 0298-53-4655.

E-mail address: kitamura.yutaka.fm@u.tsukuba.ac.jp

Abstract

With the development of CO_2 capture technologies, the cryogenic approach provides a promising alternative for greenhouse effect mitigation. In previous work, a novel CO_2 capture process was developed based on Stirling coolers (SC). However, the properties of frosted CO_2 that deposits onto the heat exchanger of SC are not completely understood but it plays an important role as a heat transfer medium and affects subsequent CO_2 deposition. In order to improve the system performance and capture efficiency, a thorough analysis of the CO_2 frost process becomes especially significant. Based on this aim, numerical and experimental analysis of CO_2 frost formation in the cryogenic capture process has been investigated in the present work. The results show that the frosted CO_2 layer significantly influences the heat transfer between the gas stream and cooling fins. Over time (from 0 to 60 min), the thickness of the frost layer increased from 0 to 3.0 mm. The thermal conductivity increased from 0 to 0.4 W/(m·K). When the flow rate was set at 1 L/min, the temperature of the cold head of the SC varied from -105.2 ℃ to -102.1 ℃. When the flow rate was 3 L/min, the temperature rose from -106.3 ℃ to -98.0 ℃.

Keywords: CO_2 capture, cryogenic, frost layer, thickness, thermal conductivity

Nomenclature

T_a	Temperature of ambient, ℃
T_g	Temperature of flue gas, ℃
T_f	Temperature of frost layer, ℃
t_1	Idle operating time, min
t_2	Capture time, min
Greek letters	
v	Flow rate of flue gas, L/min
λ_c	Thermal conductivity for individual unit volume, W/(m·K)
λ_f	Effective thermal conductivity of frost layer, W/(m·K)
ρ_f	Density of frost, kg/m^3
ω_a	Humidity of ambient, %
δ_f	Thickness frost layer, mm
Abbreviations	
CCS	CO_2 capture and storage
SC	Stirling cooler
FGD	Flue gas desulphurization
ESP	Electrostatic precipitators
SCR	Selective catalytic reduction

1. Introduction

CO_2 capture and storage (CCS) is proposed as an important strategy to help mitigate the increasing serious issue of global warming. CCS consists of three steps: capture, transport and storage. Of these three steps, CO_2 capture has attracted the most attention due to the technical challenges associated with its implementation. Currently, the main CO_2 capture technologies contain chemical absorption, membrane separation, cryogenic distillation and physical adsorption. Among these technologies, amine based absorption is the most technically mature and commercially viable to be integrated into coal-fired power plants (Liang et al., 2011). The main advantages of this technology are that it can be retrofitted to existing power plants and other industrial stations with minimum modification. Furthermore, amine scrubbing is suitable for low CO_2 partial pressure in flue gas (Luis et al., 2012). However, there are still some drawbacks: 1) the energy consumption required for regeneration; 2) the corrosion of the installations; 3) the environmental impact (Davison, 2007; Huang et al., 2011). For this reason, various research has been carried out on the improvement of existing technologies and the exploitation of novel processes.

Cryogenic CO_2 separation technology is attracting increased attention due to its significance in recent years. As a promising alternative, this technology has several advantages: 1) to avoid the energy penalty in the regeneration process; 2) to prevent

the issue of corrosion caused by solvent; 3) to realize a CO_2 capture method that is environmental friendly without causing degradation. In previous work (Song et al., 2012a), a novel CO_2 capture process based on Stirling coolers (SC) was exploited. The whole system is chilled by SCs, and the moisture and CO_2 in flue gas were captured at different places. Simultaneously, the residual gas (such as N_2) passes through the system without phase change. The core part of the process is that CO_2 in the flue gas is captured in solid form. When exposed to the heat exchanger under the frost point of CO_2, the CO_2 in the gas stream will anti-sublimate and frost on the surface of the cold head. With the purpose of enhancing capture efficiency, intensive study on CO_2 frost properties is an imperative task.

Frost formation is a common phenomenon that exists in various fields, such as cryosurgery, meteorology, agriculture, aerospace industry, refrigeration industry, civil engineering (Lee and Ro, 2005). The investigation of the frost process in different engineering processes has been widely implemented (Seker et al., 2004; Kim et al., 2009; Schmelzer, 2003). It is worth noting that in spite of this a relatively large amount of literature has investigated the frost formation process, however most relate to moisture and there are still gaps and inconsistencies (O'Neal and Tree, 1985). Reports with respect to the frosting process of CO_2 in the greenhouse gas control field are few (Shchelkunov et al., 1986; Sumarokov et al., 2003). According to Ogunbameru et al. in

1973, the frost behavior of CO_2 is different from moisture. In the moisture frost process, the density increases continuously with the total mass of the deposition (Na and Webb, 2004a). By contrast, the initial increase rate in density for the frosted CO_2 is large but in the later stages it decreased (Brian et al., 1969). Meanwhile, the thermal conductivity of solid CO_2 is related to the variation of the layer density (Cook and Davey, 1976). Therefore, the frost formation of CO_2 is an intricate deposition process. In light of these characteristics, it is necessary to investigate the CO_2 frost formation process in order to improve cryogenic CO_2 capture performance.

The objective of this work is to numerically analysis the properties of the CO_2 frost formation process by the SC based cryogenic CO_2 capture technology. In order to achieve this aim, the influence of the frost layer on thermal conductivity and temperature variation has also been investigated in detail. Moreover, the variation of the frost layer thickness has been simulated.

The paper is organized as follows: First, the base case of CO_2 capture is described. Then the whole frost formation process is explained in three sections. Subsequently, the experimental conditions and the structure of the heat exchanger for CO_2 frost are introduced. Finally, the variation of frost layer (thickness and thermal conductivity) and temperature in the capture process is simulated and analyzed in detail.

2. Base case

The schematic of the exploited CO_2 capture process is shown in Fig. 1. The whole capture process can be described as follows: Prior to CO_2 recovery, the gas stream from the combustion furnace flows through the removal units. There the acid gases (such as SO_x and NO_x) and particulate can be separated as they affect the capture performance and installation. SO_x removal is usually achieved in a flue gas desulphurization (FGD) unit. Particulate matter such as fly ash is removed by electrostatic precipitators (ESP). NO_x is removed using selective catalytic reduction (SCR). Then, the gas mixture is fed to the developed cryogenic capture system which is mainly composed of three SCs. By the first SC, the flue gas is chilled to (between 40 and 50 ℃) from a high initial temperature (around 60 ℃ after desulphurization). The function of this section is to decrease the mechanical shock of the gas stream to the installation. It should be pointed out that as the temperature of the flue gas decreases rapidly to the freezing point of H_2O, the moisture in the gas condenses and is recovered at the condensate water outlet. After the pre-chilling step, the gas stream is introduced into the CO_2 separation tower. In this section, the CO_2 in the flue gas frosts onto the heat exchanger of the SC-2 under the cryogenic condition (around -105 ℃) and the residual gas (mainly as N_2) is exhausted without phase change. In this way, the CO_2 is recovered from flue gas. In the last step, the captured CO_2 is stored in the column chilled by SC-3 to avoid sublimation. Furthermore, since the temperature of

residual gas and condensate water is low, it can be used to cool down the follow-up gas stream by heat exchanger for energy conservation. In addition, the flue gas in our research is simulated by synthetic gas (N_2/82 vol.%, CO_2/13 vol.% and H_2O/5 vol.%). After the cryogenic CO_2 capture process, the composition of the residual gas is N_2/99.38 vol.% and CO_2/0.62 vol.%. Furthermore, the average flow rates of the initial and final gas stream are 3 L/min and 2.47 L/min, respectively. The details of the capture process can be found in previous work (Song et al., 2012a).

3. CO_2 frost formation process

As mentioned in the relevant research, the whole CO_2 frost formation process can be divided into three periods (Hayashi et al., 1977). 1) Crystal growth period. 2) Frost growth period. 3) Frost formation period. The sketch of the frost formation process is depicted in Fig. 2.

3.1 Crystal growth period

This is a relatively short period during the early stage of the frosted CO_2 formation process. At the beginning, the CO_2 in the flue gas anti-sublimates into small crystals and is simultaneously extracted from the gas stream by frosting onto the cooling fin of the heat exchanger. The frosted CO_2 plays a role as the nucleus for further crystallization. New CO_2 crystal grows on the previous nucleus and spreads in all

directions. It needs to be pointed out that this period has a significant influence on the further frost growth process. However, the characteristics of this period are complexity and instantaneity. Therefore, the effect of this period on the whole capture performance is taken into account by setting appropriate initial parameters (Cui et al., 2011).

3.2 Frost growth period

The frost growth period is characterized by a porous frost structure growing. The structure consists of solid CO_2 (99.89 mol.%), a small quantity of residual gas (around 0.04 mol.%) and a trace of H_2O (approximate 0.07 mol.%). Thus, in this period, the frost layer becomes visibly rugged due to new crystal formation on the surface. The subsequent CO_2 crystal leads to further growth and densification of the frost layer. The thickness of the frost deposition increases rapidly.

3.3 Frost densification period

In the last period, the frost formation is fully developed. The increasing rate of deposition slows and the density increases gradually. As the frost layer grows, the heat resistance of the frost layer also rises. This reflects in the decrease in the effective thermal conductivity of the cold head and causes a surface temperature increase. When the temperature of the frost layer surface becomes higher than the freezing point, the

CO_2 in the subsequent gas stream cannot frost. Meanwhile, the following feed gas can cause that part of the frosted CO_2 on the layer surface to sublimate. The sublimation results in a thinning layer, and then enhances the thermal conductivity of the layer. The CO_2 in the gas stream frosts again until a dynamic equilibrium of anti-sublimation and sublimation of the whole frost process is achieved.

4. Materials and methods

4.1 Materials

In order to measure the temperature distribution, eight K-type thermocouples were placed on different places in the system, and all the thermocouples are connected to a data-acquisition system. Commercial software is used to record and process data in a database format using a computer. The temperature data measured by the thermocouples is recorded every 0.1 s during the total testing time. The ambient temperature (T_a) and humidity (ω_a) are measured with the thermo hygrometer in the laboratory. All the heat exchangers in the system are made from copper. The structure of the heat exchanger of SC-2 is shown in Fig. 4(a). The details of its size are described in Fig. 4(b). The length and diameter of the cold head are 230.0 and 36.0 mm, respectively. The length and width of the cooling fin are 15.0 and 1.0 mm, respectively. The interval between the fins is 6.0 mm.

4.2 Methods

The formation of the frost layer has a significant influence on the performance of the whole capture process. In order to investigate the variation of the frost layer in the CO_2 capture process, two parameters are considered to represent the characteristics of variation, namely thickness (δ_f) and thermal conductivity (λ_f).

The thickness of the frost layer is a significant parameter that reflects the properties of the frost process. Its variation process is observed by use of a charge coupled device (CCD) camera. Simultaneously, tick marks are added among the cooling fins of the cold head to facilitate thickness measurement. It is obvious that the deposited frost layer will lead to an increase in thermal resistance. Meanwhile, it influences the heat flux between the cold head of SC-2 and the gas stream, and results in the decrease of capture efficiency. Thus, in order to evaluate the characteristic of the frost layer, the investigation of effective thermal conductivity (λ_f) is necessary. The detail calculation method is described as follows (Lenic et al., 2009):

$$\lambda_f = \frac{\delta_f}{\sum_{c=1}^{\delta} \frac{1}{\lambda_c}} \tag{1}$$

where δ_f represents the thickness of the frost layer. λ_c represents the coefficient of the thermal conductivity for individual unit volume.

4.3 Model of CO_2 frost process

According to previous discussion, knowledge of the characteristics of CO_2 frost is important to improve the capture performance and decrease the energy penalty of the cryogenic system. In order to simplify the intricate CO_2 frost process, some assumptions are mentioned as follows: 1) the water in the frost layer is neglected due to its fractional content. 2) the density of the frost layer on the heat exchanger is homogeneous. 3) radiation effect within the frost layer is negligible.

The CO_2 frost process on the cold surface is simulated in Fig. 3. The mass and heat transfer processes have been introduced in our previous work (Song et al., 2012b). The thermal dynamic behavior of the frosted CO_2 layer is described using empirical models. The summaries of the frost density (ρ_f) and thickness (δ_f) correlation model are listed in Tables 1 and 2. The correlations published in the literature for thermal conductivity (λ_f) calculations are shown in Table 3.

5. Results and discussion

5.1 Frost layer

5.1.1 Growth of the frost layer

When the temperature dropped to the freezing point of CO_2, the flue gas was loaded

into the system. Initially, there was no frost present on the heat exchanger (as shown in Fig. 5a). As time went on, the frost began to form, temperature increased and the crystals of frosted CO_2 became gradually larger (as shown in Fig. 5b). Then, as the crystal of solid CO_2 gathered, frost grew on the heat exchanger and its volume expanded rapidly (as shown in Fig. 5c). At the full growth stage, the captured CO_2 almost totally covered the cooling fin of the heat exchanger (as shown in Fig. 5d).

The effect of the gas flow rate on the thickness of the frost layer is shown in Fig. 6. The result indicates that the thickness of the frost layer increased continuously with time however the rate of deposition was not constant. Initially, the growth rate was slow and then increased rapidly. That can be explained by the fact that during the stage of crystal growth (described in section 3.1), the variation in deposition was moderate. When the CO_2 crystal covered the cooling fin, the growth rate of the frost layer accelerated. In the frost formation period, the frost layer increased sufficiently. Meanwhile, the rate of frost deposition decreased again and eventually approached zero. In this period, the variation of the frost layer mainly presented in density. After 60 minutes, the thickness of frost layer reached 3.0 mm. Additionally, it can also be seen that along with the increase in the flow rate, the thickness of the frosted CO_2 grew accordingly.

5.1.2 Thermal conductivity of the frost layer

The influence of the flow rate for the gas stream on the thermal conductivity (λ_f) of the frost layer is shown in Fig. 7. From the results, it indicates that the thermal conductivity increased with capture time passed. At the beginning of the capture process, the effective conductivity of the frost layer increased quickly, and with time decelerated. In addition, with the increase in the flow rate of feed gas, the increase rate of the thermal conductivity obviously accelerated. It is worth noting that after 20 minutes the variation of the thermal conductivity of the frost deposition amplified slowly, and reached around 0.4 W/(m·K) after 60 min. This can be explained by the fact that the rise in thermal conductivity with time is due to the variation of the thickness and density of the frost layer. At the initial period (from 0 to 20 min), the CO_2 crystals deposited on the surface of the cold head and the growth rate of frost layer was fast. Consequently, the thermal conductivity increased and the rate was also fast. At a subsequent time (from 20 to 60 min), more CO_2 crystal groups formed around the existing crystals and the gas pores were filled up. The solid phase became denser through internal diffusion. However, the variation of the thickness for the frost layer slowed down. Therefore, the increase rate in the thermal conductivity decelerated.

5.2 Temperature variation

As the frosted CO_2 layer grows, a gradual increase in the frost surface temperature

occurs due to the augmentation of heat resistance which is unfavorable to the capture process. This is because the temperature driving force is reduced due to the frost insulation on the heat exchanger surface, and hence energy and mass transfer rates drop. As a consequence, this results in a decrease of CO_2 capture efficiency.

Fig. 8 indicates that SC-1 has a significant influence on the temperature of SC-2, and impacts the whole capture performance. During the capture process, SC-1 played a part in pre-chilling the flue gas and preventing the rapid increase of the temperature in the capture tower. The temperature of SC-2 is lower when SC-1 is working compared to stop.

Fig. 9 indicates the influence of flue gas flow rate on the temperature of SC-2. At the initial stage of gas inflow, the temperature of the heat exchanger of SC-2 increased quickly. As the frost layer formed on the surface of the cold head, the increase in speed trended to constant. From the results, it can be concluded that if flow rate was controlled slightly, the lower the temperature in the system can be maintained. This is because a high flow rate would lead to a high increase speed in the CO_2 frost layer. Due to the frost point of CO_2 being far above the temperature of the heat exchanger, when the frost formed, the temperature of the heat exchanger increased rapidly. Along with the increase in flow rate, the temperature change also increased gradually.

The influence of temperature variation of SC-1 on the properties of the frost layer is

investigated in Fig. 10 and 11. In Fig. 10, with the decrease in the temperature of SC-1, the rate of frost growth increases. When the temperature of SC-1 was set to -20 ℃, the frost deposited slowly during the initial 20 minutes. Then the layer grew rapidly in the following 20 minutes. Finally, the rate of deposition decreased again and tended to zero. This is because during the initial 20 minutes, the CO_2 formed crystals on the surface of the cold head. Therefore, the frost layer changed slightly. From the 20 minute mark, the CO_2 crystal fully covered the surface of the cold head and the density of frost layer grew rapidly. When the frost layer had increased sufficiently, the rate decreased again from the 40 minutes mark. With the decreasing temperature of SC-1, the crystal formation stage became shorter and the rate of deposition faster. When the temperature dropped down to -60 ℃, the variation of frost thickness stabilized after 30 minutes. In Fig. 11, at the initial period the thermal conductivity was almost zero due to little frosted CO_2 on the cold head. While capture time passed, the heat transfer coefficient of the frost layer increased rapidly but the increase rate decelerated due to the decrease in the densification rate. After 60 minutes, the thermal conductivity of deposited CO_2 was around 0.4 W/(m K). Meanwhile, with the decrease in temperature of SC-1, the thermal conductivity of the deposition increased. That is because the lower temperature of SC-1 facilitates the pre-chilling of the flue gas, and CO_2 solidification onto the cold surface.

6. Conclusion

Frost formation is a vital consideration in cryogenic CO_2 capture technology, and the phenomenon of CO_2 frosts on the surface of the heat exchanger has an important influence on capture performance. Based on this, the growth processes of the CO_2 frost layer and its effect on temperature variation have been numerically analyzed in this paper. The effect of frost layer growth on thermal conductivity and temperature variation was also investigated. According to the results of simulation and experiments, the following conclusions are given:

- The thickness of the frost layer increased with time but the rate of CO_2 deposition decreased gradually. Furthermore, with the increase in the flow rate, the frost growth also accelerated. After 60 minutes, the thickness of frost layer was 3.0 mm.
- The thermal conductivity of the frost layer increased due to the growth of the frost layer. Nevertheless, as time passed, its increase rate reduced. After 60 minutes, the thermal conductivity of the frost layer increased to around 0.4 W/(m·K).
- The frost surface temperature increased rapidly as frost insulated the heat exchanger. Meanwhile, with the decrease in the flow rate, the increase rate of temperature decelerated. When the flow rate was set at 1 L/min, the temperature

of the cold head for the SC varied from -105.2 ℃ to -102.1 ℃ after 60 minutes. When the flow rate was 3 L/min, the temperature rose from -106.3 ℃ to -98.0 ℃. However, the rate of the increase declined and approached zero when the energy balance between the gas stream and frost layer was reached.

Acknowledgement

This research is supported by Adaptable and Seamless Technology transfer Program through the target driven R&D (AS2115051D) of the Japan Science and Technology Agency (JST). We thank Mr. Yamano and Mr. Yamasaki of Tanabe Engineering Corporation for their help with technology.

References

Brian, P.L.T., Reid, R.C., Brazinsky. I., 1969. Cryogenic frost properties. Cryogenic Technology 5, 205.

Cook, T., Davey, G., 1976. The density and thermal conductivity of solid nitrogen and carbon dioxide. Cryogenics 363-369.

Cui, J., Li, W.Z., Liu, Y., Jiang, Z.Y., 2011. A new time- and space-dependent model for predicting frost formation. Applied Thermal Engineering 31, 447-457.

Davison, J., 2007. Performance and costs of power plants with capture and storage of CO_2. Energy

32, 1163-1176.

Hayashi, Y., Aoki, K., Yuhara, H., 1977. Study of frost formation based on a theoretical model of the frost layer. Heat Transfer - Japanese Research 6, 79-94.

Huang, Y., Wang, M., Stephenson, P., Rezvani, S., McIlveen-Wright, D., Minchener, A., Hewitt, N., Dave, A., Fleche, A., 2011. Hybrid coal-fired power plants with CO_2 capture: A technical and economic evaluation based on computational simulations. Fuel, doi:10.1016/j.fuel.2010.12.012.

Kim, K.H., K, H.J., Kim, K., Kim, Y.W., Cho, K.J., 2009. Analysis of heat transfer and frost layer formation on a cryogenic tank wall exposed to the humid atmospheric air. Applied Thermal Engineering 29, 2072-2079.

Lee, K., Jhee, S., Yang, D., 2003. Prediction of the frost formation on a cold flat surface. International Journal of Heat Mass Transfer 46, 3789-3796.

Lee, Y.B., Ro, S.T., 2005. Analysis of the frost growth on a flat plate by simple models of saturation and supersaturation. Experimental Thermal and Fluid Science 29, 685-696.

Lenic, K., Trp, A., Frankovic, B., 2009. Transient two-dimensional model of frost formation on a fin-and-tube heat exchanger. International Journal of Heat and Mass Transfer 52, 22-32.

Liang, H., Xu, Z., Si, F., 2011. Economic analysis of amine based carbon dioxide capture system with bi-pressure stripper in supercritical coal-fired power plant. International Journal of Greenhouse Gas Control 5, 702-709.

Luis, P., Van Gerven, T., Van der Bruggen, B., 2012. Recent developments in membrane-based

technologies for CO_2 capture. Progress in Energy and Combustion Science 38, 419-448.

Na, B., Webb, R.L., 2004a. Mass transfer on and within a frost layer. International Journal of Heat and Mass Transfer 47, 899-911.

Na, B., Webb, R.L., 2004b. New model for frost growth rate. International Journal of Heat and Mass Transfer 47, 925-936.

Ogunbameru, A.N., Brian, P.L.T., Reid, R.C., 1973. On carbon dioxide frost formation. Industrial & Engineering Chemistry Fundamentals 12, 385-387.

O'Neal, D.L., Tree, D.R., 1985. A review of frost formation in simple geometries. ASHRAE Transactions 91,267-272.

Sahin, A.Z., 2000. Effective thermal conductivity of frost during the crystal growth period. International Journal of Heat and Mass Transfer 43, 539-553.

Sanders, C.T., 1974. Frost formation: the influence of frost formation and defrosting on the performance of air coolers, Ph. D. thesis, Technische Hogeschool, Delft, The Netherlands.

Schmelzer, J.W.P., 2003. Kinetic and thermodynamic theories of nucleation. Materials Physics and Mechanics 6, 21-33.

Seker, D., Karatasa, H., Egrican, N., 2004. Frost formation on fin-and-tube heat exchangers. Part I-Modeling of frost formation on fin-and-tube heat exchangers. International Journal of Refrigeration 27, 367-374.

Shchelkunov, V.N., Rudenko, N.Z., Shostak, Y.V., Dolganin, V.I., 1986. Surface desublimation of

carbon dioxide from binary gas mixtures. Translated from Inzhenerno-Fizicheskii Zhurnal 51 (6), 965-970.

Song, C.F., Kitamura, Y., Li, S.H., Ogasawara, K.J., 2012a. Design of a cryogenic CO_2 capture system based on Stirling coolers. International Journal of Greenhouse Gas Control 7, 107-114.

Song, C.F., Kitamura, Y., Li, S.H., 2012b. Evaluation of Stirling cooler system for cryogenic CO_2 capture. Applied Energy 98, 491-501.

Sumarokov, V.V., Stachowiak, P., Jezowski, A., 2003. Low-temperature thermal conductivity of solid carbon dioxide. FIzika Nizkikh Temperatur 29 (5), 603-605.

Woodside, W., 1958. Calculation of the thermal conductivity of porous media. Canadian Journal of Physics 36,815-23.

Figures Captions:

Fig. 1 Schematic diagram of the SC based cryogenic CO_2 capture process

Fig. 2 Sketch diagram of CO_2 frost formation process. (1) Crystal growth period. (2) Frost growth period. (3) Frost densification period (Cui et al., 2011)

Fig. 3 The growth process of the CO_2 frost layer on the heat exchanger of SC-2. The difference in color represents the direction of the increase in density of the frost layer (from blue to red)

Fig. 4 The structure (a) and dimension (b) of the heat exchanger for capturing CO_2

Fig. 5 CO_2 frosting process: (a) no frost; (b) initial frost; (c) growth of the frost; (d) full growth

Fig. 6 Effect of the flow rate on thickness of the CO_2 frost layer. (T_{SC-1}= -30 ℃; T_{SC-2}= -120 ℃; T_{SC-3}= -120 ℃; t_1=240 min; t_2=60 min)

Fig. 7 Effect of the flow rate on thermal conductivity (λ_f) of the CO_2 frost layer. (T_{SC-1}= -30 ℃; T_{SC-2}= -120 ℃; T_{SC-3}= -120 ℃; t_1=240 min; t_2=60 min)

Fig. 8 Effect of SC-1 on the temperature variation of the SC-2's cold head. (T_{SC-1}= -30 ℃; T_{SC-2}= -120 ℃; T_{SC-3}= -120 ℃; ν=2 L/min; t_1=240 min; t_2=60 min)

Fig. 9 Effect of flow rate on the temperature variation of SC-2's cold head. (T_{SC-1}= -30 ℃; T_{SC-2}= -120 ℃; T_{SC-3}= -120 ℃; t_1=240 min; t_2=60 min)

Fig. 10 Effect of temperature variation of SC-1 on the thickness of the frost layer. (T_{SC-2}= -120 ℃; T_{SC-3}= -120 ℃; ν=2 L/min; t_1=240 min; t_2=60 min)

Fig. 11 Effect of temperature variation of SC-1 on the thermal conductivity of the frost layer. (T_{SC-2}= -120 ℃; T_{SC-3}= -120 ℃; ν=2 L/min; t_1=240 min; t_2=60 min)

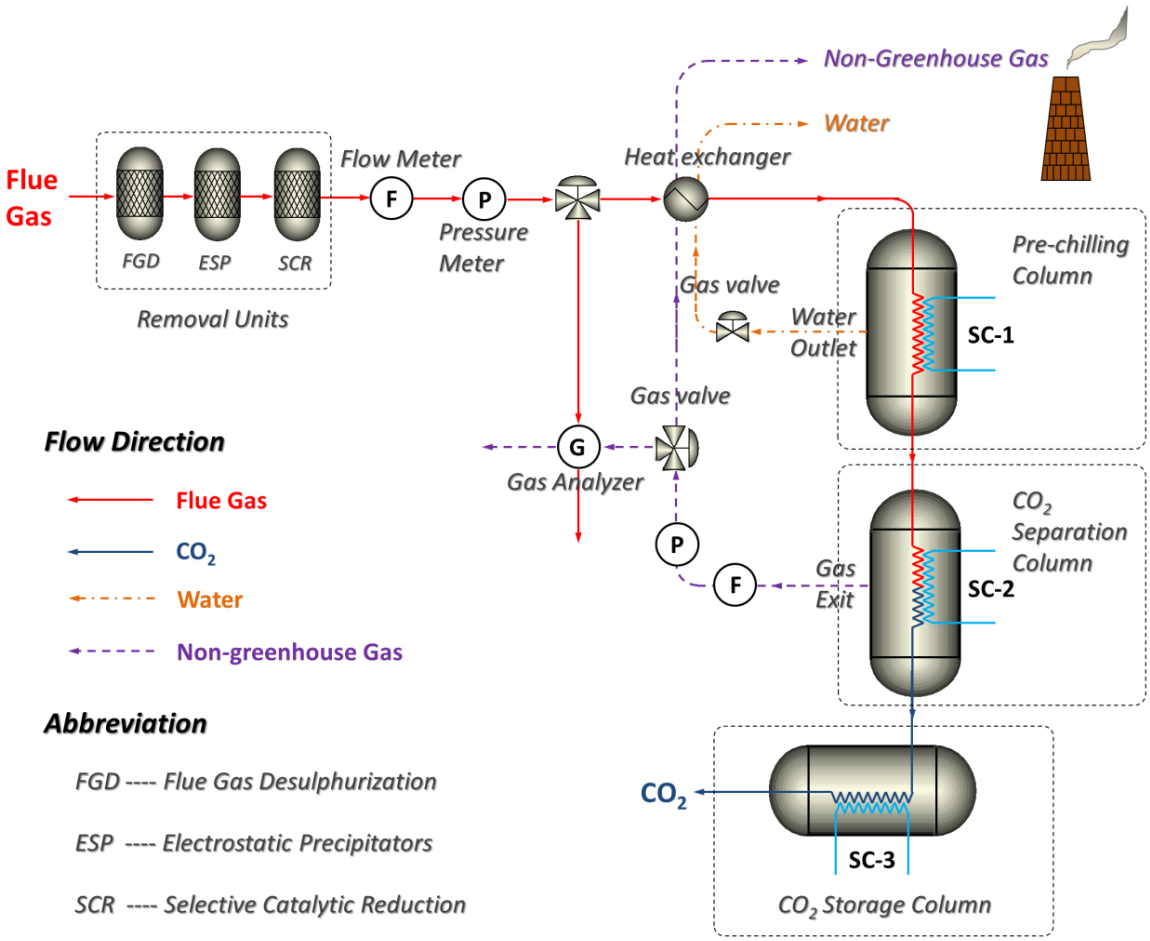

Fig. 1 Schematic diagram of the SC based cryogenic CO_2 capture process

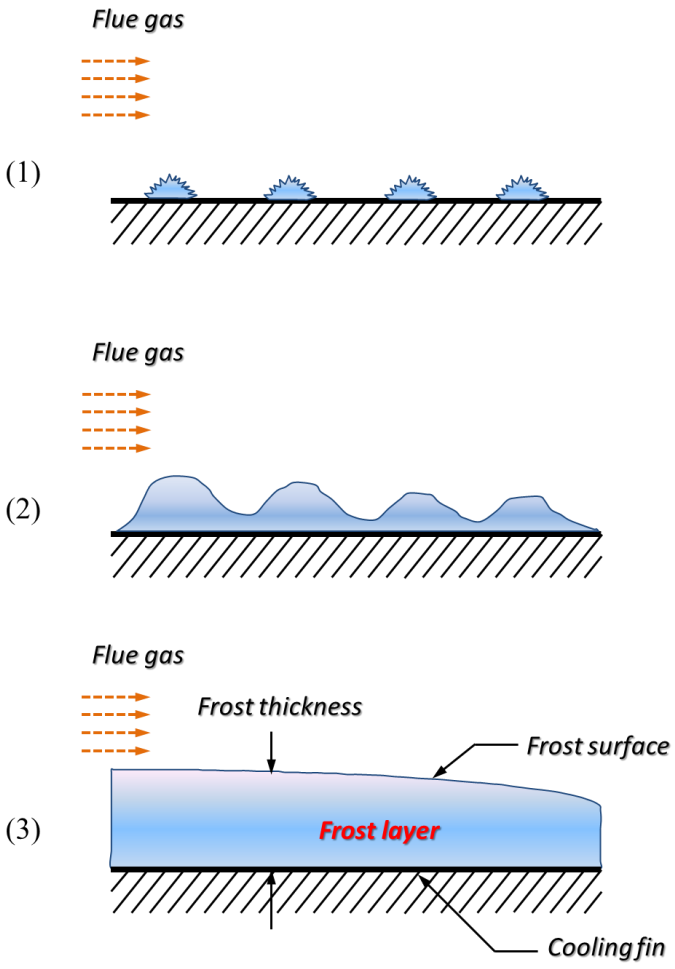

Fig. 2 Sketch diagram of CO_2 frost formation process. (1) Crystal growth period. (2) Frost growth period. (3) Frost densification period (Cui et al., 2011)

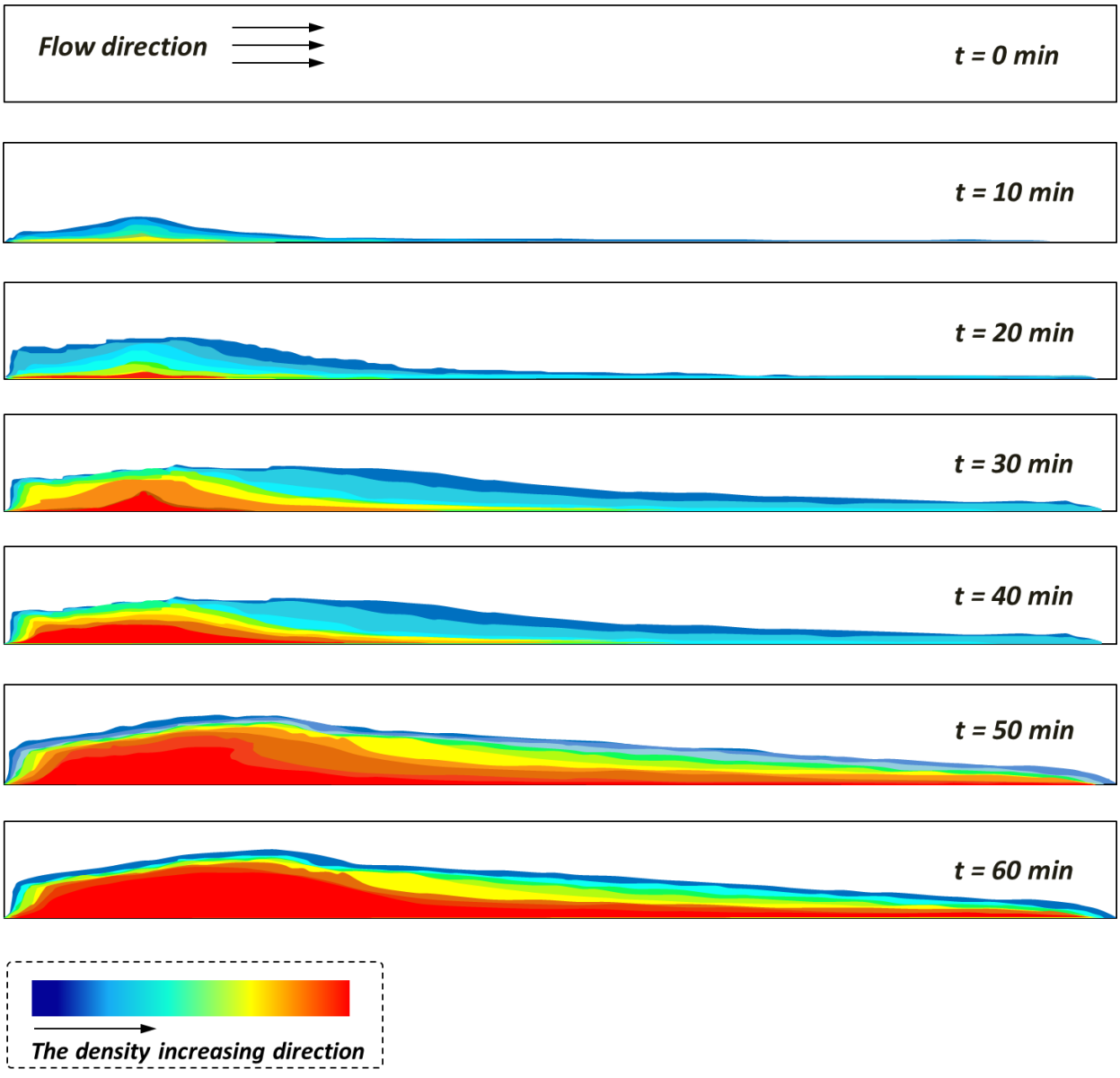
Flow direction
t = 0 min
t = 10 min
t = 20 min
t = 30 min
t = 40 min
t = 50 min
t = 60 min
The density increasing direction

Fig. 3 The growth process of the CO_2 frost layer on the heat exchanger of SC-2. The difference in color represents the direction of the increase in density of the frost layer (from blue to red)

(a)

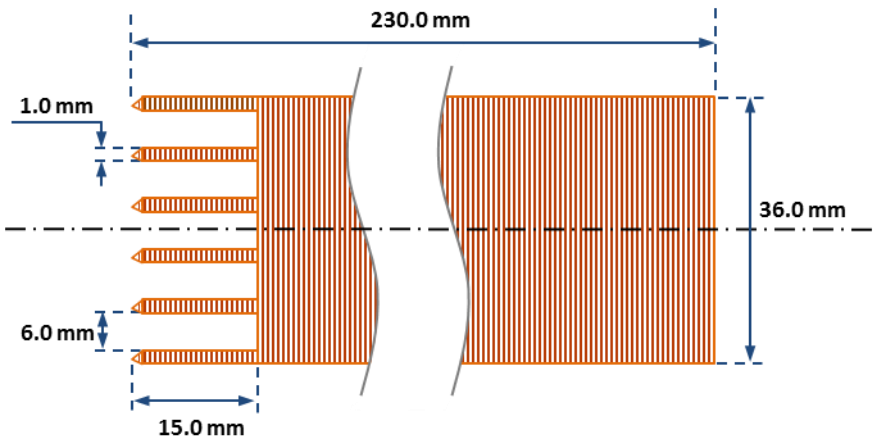

(b)

Fig. 4 The structure (a) and dimension (b) of the heat exchanger for capturing CO_2

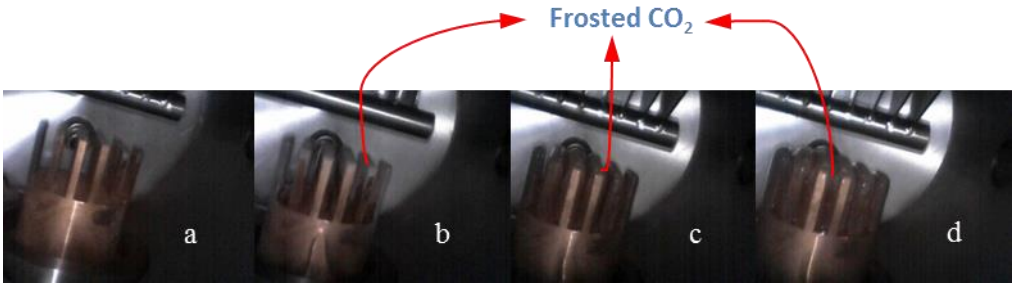

Fig. 5 CO_2 frosting process: (a) no frost; (b) initial frost; (c) growth of the frost; (d) full growth

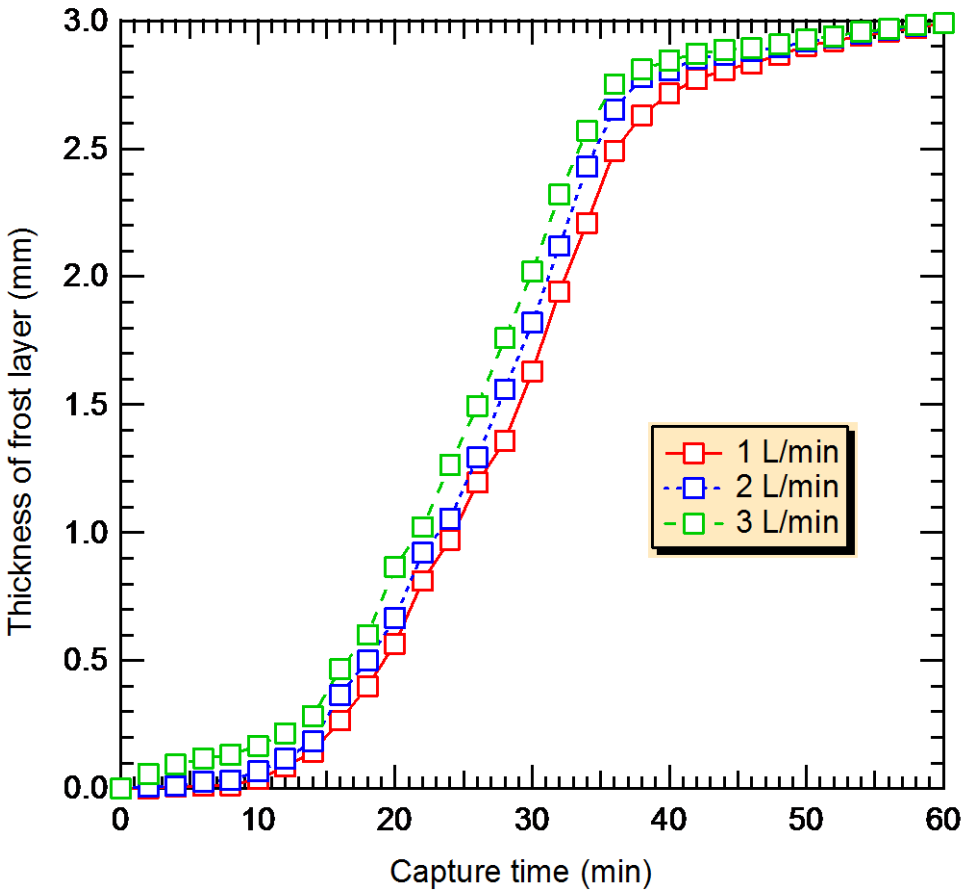

Fig. 6 Effect of the flow rate on thickness of the CO_2 frost layer. (T_{SC-1}= -30 ℃; T_{SC-2}= -120 ℃; T_{SC-3}= -120 ℃; t_1=240 min; t_2=60 min)

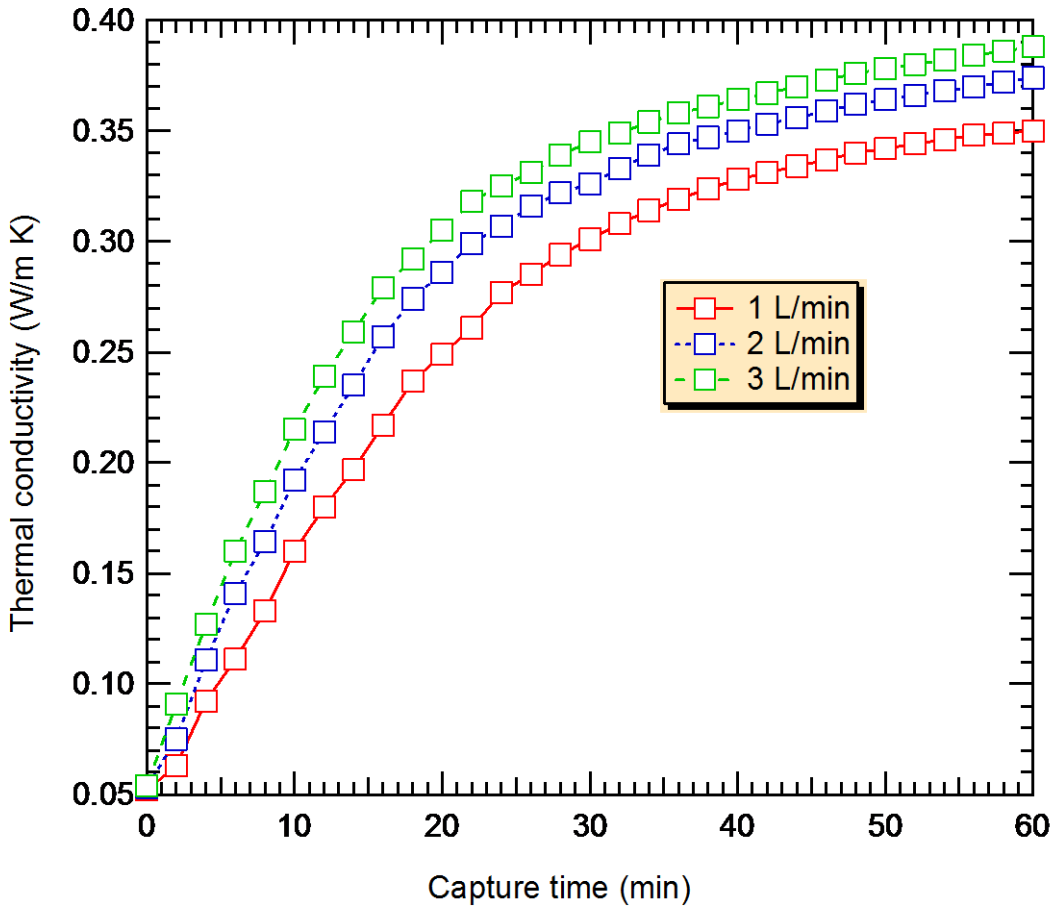

Fig. 7 Effect of the flow rate on thermal conductivity (λ_f) of the CO_2 frost layer. (T_{SC-1}= -30 ℃; T_{SC-2}= -120 ℃; T_{SC-3}= -120 ℃; t_1=240 min; t_2=60 min)

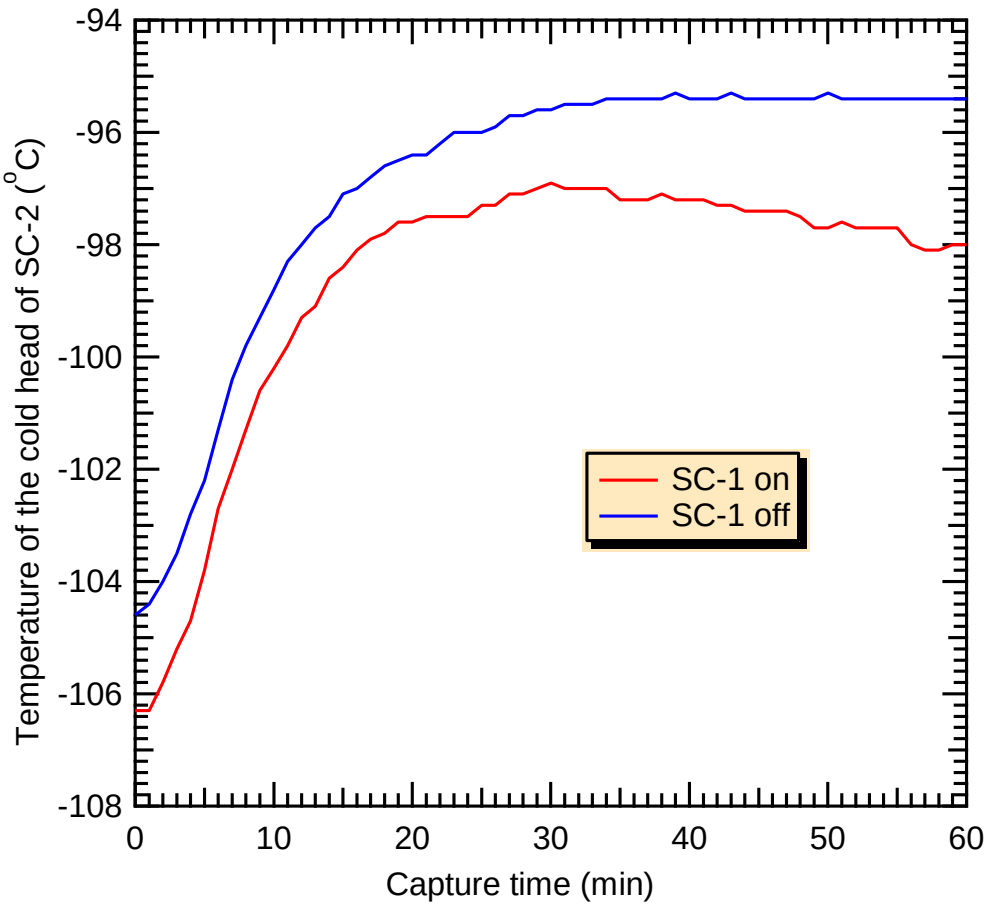

Fig. 8 Effect of SC-1 on the temperature variation of the SC-2's cold head. (T_{SC-1}= -30 ℃; T_{SC-2}= -120 ℃; T_{SC-3}= -120 ℃; v=2 L/min; t_1=240 min; t_2=60 min)

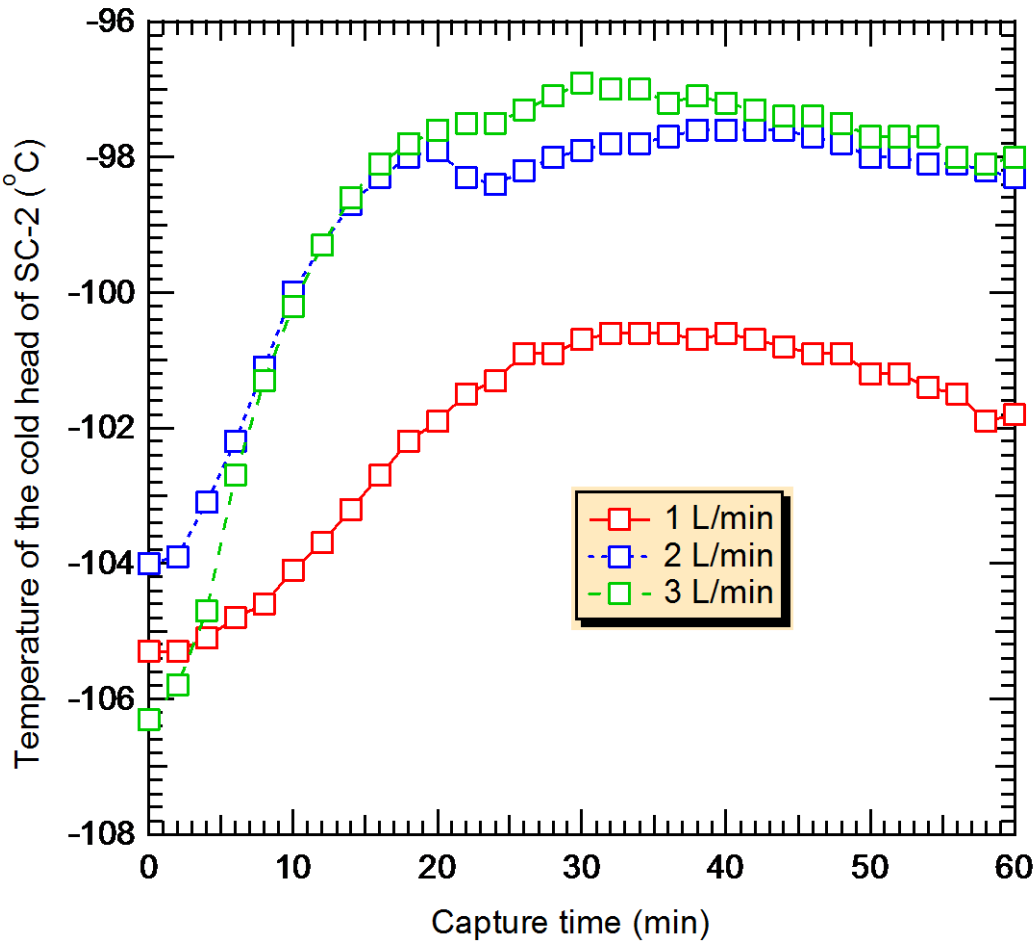

Fig. 9 Effect of flow rate on the temperature variation of SC-2's cold head. (T_{SC-1}= -30 ℃; T_{SC-2}= -120 ℃;

T_{SC-3}= -120 ℃; t_1=240 min; t_2=60 min)

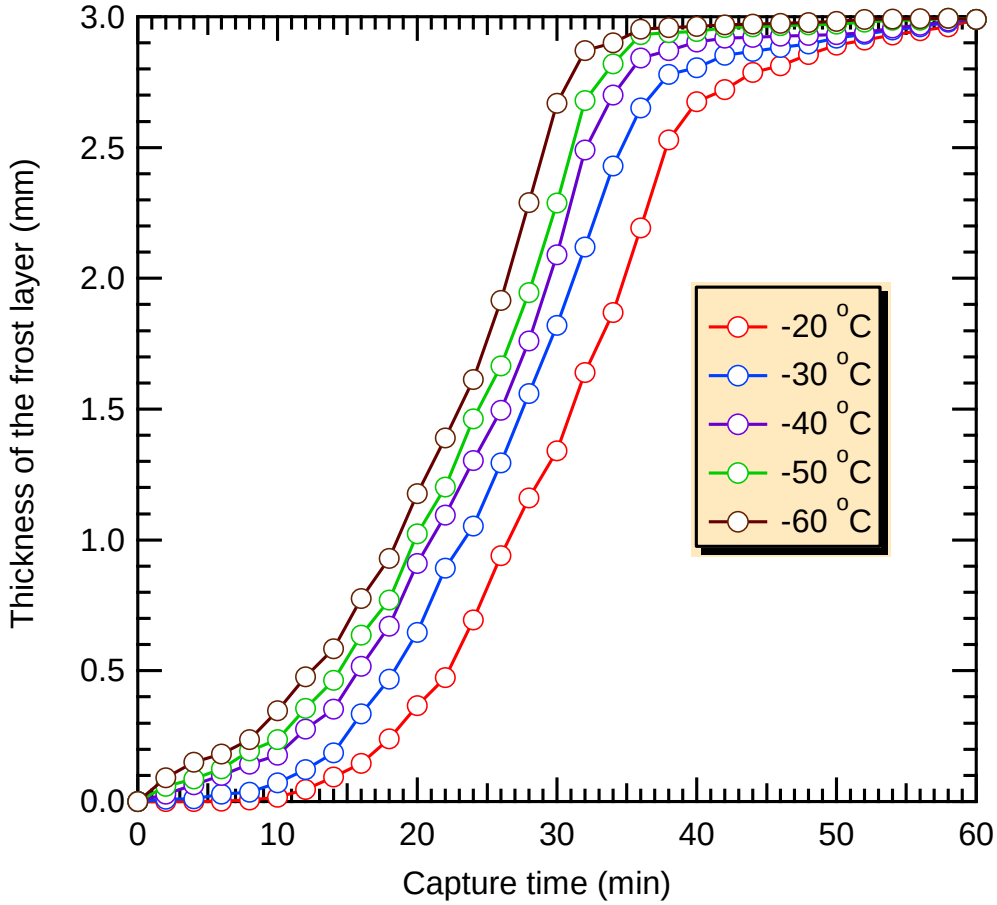

Fig. 10 Effect of temperature variation of SC-1 on the thickness of the frost layer. (T_{SC-2}= -120 ℃; T_{SC-3}= -120 ℃; v=2 L/min; t_1=240 min; t_2=60 min)

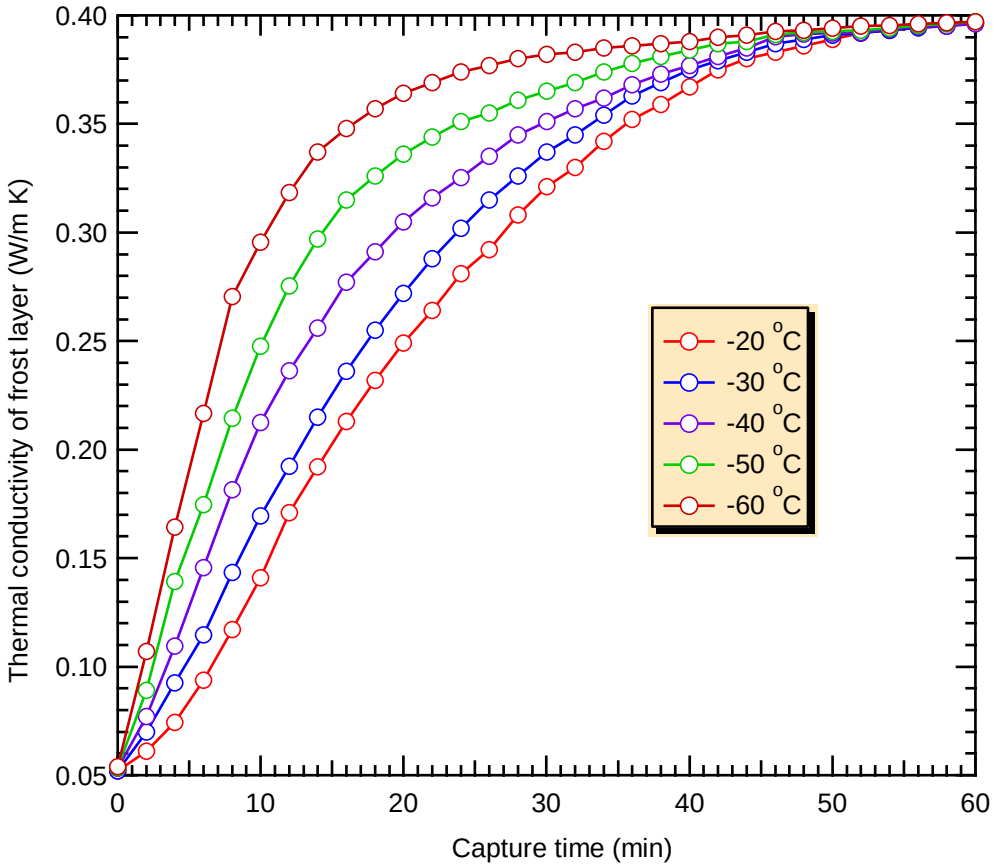

Fig. 11 Effect of temperature variation of SC-1 on the thermal conductivity of the frost layer.

(T_{SC-2}= -120 ℃; T_{SC-3}= -120 ℃; v=2 L/min; t_1=240 min; t_2=60 min)

Table Captions:

Table 1 Calculation models for the density of the frost layer.

Table 2 Empirical models for the thickness of the frost layer.

Table 3 Correlation models for the thermal conductivity of the frost layer.

Table 1

Calculation models for the density of the frost layer.

---

1) Average frost density calculated by Ogunbameru et al., 1973:

$$\rho_f = -\ln(GI / I_0) / \mu_m \cdot x$$

In which G is the dimensionless geometrical correction factor. I is number of γ-radiation counts. I_0 is number of counts without frost deposit. μ_m is mass attenuation factor. x is frost layer thickness.

2) Frost density is determined from empirical correlation by Hayashi et al., 1977:

$$\rho_f\big|_t = 650 \cdot \exp\left[0.277 \cdot T_f(t)\right]$$

3) Calculation of frost density proposed by Cui et al. in 2011:

$$\rho_f(\vec{x},t) = \rho_g \cdot \left[1-\alpha_i \cdot (\vec{x},t)\right] + \rho_i \cdot \alpha_i \cdot (\vec{x},t)$$

Where ρ_g and ρ_i are the density of gas phase and crystal, respectively. α_i is the volume fraction of frosted droplets.

4) The local density of the frost layer (Na and Webb, 2004b; Lenic et al., 2009):

$$\rho_f = \varepsilon \cdot \rho_g + (1-\varepsilon)\rho_s$$

Here ε is the local porosity of the frost layer. It is defined as following:

$$\varepsilon = \frac{\rho_s - \rho_f}{\rho_s - \rho_g}, \quad 0 \leqslant \varepsilon \leqslant 1$$

In which, ρ_g, ρ_s and ρ_f are the density of gas phase, solid phase and frost layer, respectively.

Table 2

Empirical models for the thickness of the frost layer.

1) The frost thickness for each time interval is given by Yun et al., 2002:

$$\delta_f\big|_{t+\Delta t} = \delta_f + \Delta\delta_f$$

2) The average frost thickness calculated by Cui et al., 2011:

$$\delta_f(t) = \frac{\sum_{j=1}^{n}\left[\delta_j(t)\Delta x\right]}{L}$$

In which $\delta_j(t)$ is the local thickness of frost layer. L is the length of the computational domain.

3) The average layer thickness defined by Lenic et al., 2009:

$$\delta_f = \frac{\sum_{k=1}^{M}\delta_{L,k}}{M}$$

Where $\delta_{L,k}$ is the local thickness of frost layer. M is the number of control volumes in horizontal direction.

Table 3

Correlation models for the thermal conductivity of the frost layer.

1) The total thermal conductivity is the sum of surface and inner layer. (Yun et al., 2002):

$$\lambda_{total} = \frac{\lambda_{f,s} \cdot \lambda_{f,in} \cdot (\delta_{f,s} + \delta_{f,in})}{\lambda_{f,in} \cdot \delta_{f,s} + \lambda_{f,s} \cdot \delta_{f,in}}$$

Here, the thermal conductivity of surface is given by:

$$\lambda_{f,s} = \lambda_a + \rho_{a,s} \cdot c_{p,a,s} \cdot u_a^2 \cdot C_f / 2 \cdot [y(t) + \delta_b] / 2.5$$

the thermal conductivity of inner layer is calculated by Woodside in 1958:

$$\lambda_{f,in} = \lambda_a / (1 - 6 \cdot s / \pi)^{1/3} \cdot \left\{1 - \left(c^2 - 1\right) / 2 \cdot \ln\left[(c+1)/(c-1)\right]\right\}$$

2) The frost thermal conductivity is related to temperature as a sole parameter (Sahin, 2000):

$$\lambda_f(T) = 0.131 \times 10^{-6}(1-\beta) \cdot \frac{h_s \cdot P_{atm} \cdot P_g}{T_g^{1.94} \cdot R^2 \cdot T_s^{1.06}} \cdot \exp\left[\frac{h_s}{R} \cdot \left(\frac{1}{T_g} - \frac{1}{T_s}\right)\right] + 1.202 \times 10^{-3} \beta (\rho_c)^{0.963} + (1-\beta)(1.0465 + 0.017 T_s) \times 10^{-5}$$

Where h_s is the latent heat of sublimation. P_g is the partial pressure of specific gas phase at initial temperature (T_g). T_s is the temperature of frost surface. β is the volumetric ratio of frost deposition. ρ_c is the density of crystal.

3) The empirical equation validated by Yonko and Sepsy, 1967:

$$\lambda_f = 0.024248 + 0.00072311 \rho_f + 0.000001183 \rho_f^2$$

In which ρ_f is the density of frost layer.

4) The expression demonstrated by Sanders, 1974:

$$\lambda_f = 1.202 \times 10^{-3} \cdot \rho_f^{0.963}$$

5) The correlation proposed by Lee et al., 2003:

$$\lambda_f = 0.132 + 3.13 \times 10^{-4} \cdot \rho_f + 1.6 \times 10^{-7} \cdot \rho_f^2$$